PCCP

ROYAL SOCIETY OF CHEMISTRY

PAPER

View Article Online
View Journal | View Issue

Cite this: *Phys. Chem. Chem. Phys.*, 2020, **22**, 21119

Low-power STMAS – breaking through the limit of large quadrupolar interactions in high-resolution solid-state NMR spectroscopy†

Ivan Hung * and Zhehong Gan

Received 12th August 2020,
Accepted 15th September 2020

DOI: 10.1039/d0cp04274a

rsc.li/pccp

An STMAS NMR experiment requiring significantly lower rf fields is presented, allowing acquisition of high-resolution spectra for half-integer spins regardless of the magnitude of their quadrupolar interaction. The experiment relies on frequency crossings induced by sample spinning during 'long' rf pulses to coherently cover the satellite-transitions efficiently.

Introduction

Understanding the relationship between atomic structure and function or other macroscopic properties is important to many areas of science. Solid-state nuclear magnetic resonance (NMR) spectroscopy is a powerful tool for the study of structure and dynamics at the atomic level in non-liquid samples. However, the information content available from NMR depends very strongly on the ability to resolve distinct sites in the compounds of interest and low resolution is particularly problematic for nuclei with spin quantum numbers $S > 1/2$, which make up most of the NMR-active nuclei in the Periodic Table. These nuclei have quadrupole moments that interact with their surrounding electric field gradients (EFG) leading to anisotropic line broadening, spectral overlap and loss of resolution from the quadrupolar interaction (QI). For half-integer quadrupolar nuclei (S = 3/2, 5/2, 7/2, 9/2), a broadening from the anisotropic second-order QI remains under magic-angle spinning (MAS), therefore NMR methods have been developed to regain isotropic resolution, such as double rotation (DOR),[1] dynamic angle spinning (DAS),[2] multiple-quantum magic-angle spinning (MQMAS),[3] and satellite-transition magic-angle spinning (STMAS).[4] Of the four methods, DOR and DAS require specialized hardware, while MQMAS and STMAS can be performed using conventional MAS probes. DOR is unique in allowing acquisition of one-dimensional (1D) high-resolution spectra directly, while the other methods achieve isotropic resolution indirectly by two-dimensional (2D) acquisition. Nonetheless, due to their applicability with commonly available probes, STMAS and particularly MQMAS have seen more widespread use.

Of the two methods, MQMAS has seen much broader usage since the experimental requirements for STMAS are much more stringent. For STMAS, the magic-angle setting and spinning speed stability are critical for the averaging of the large first-order quadrupolar broadening to the satellite-transitions (STs).[5] STMAS is also particular in being sensitive to the third-order quadrupolar effect[6] and motional broadening[7] due to observation of the STs. Nevertheless, a very appealing characteristic of STMAS is its use of only single-quantum (SQ) transitions which gives it a significant sensitivity advantage over MQMAS; factors of two to nine have been observed.[8]

Both MQMAS and STMAS rely on application of short pulses with strong rf fields ω_1 for correlation among different transitions.[9,10] The sensitivity (or efficiency) of both experiments depends critically on the ratio between ω_1 and the magnitude of the quadrupolar interaction $\omega_Q = 6\pi C_Q/[2S(2S-1)]$, where C_Q is the quadrupole coupling constant. In practice, experimental efficiency tends to be low either because C_Q is large, or the attainable ω_1 is insufficient. This is a particularly acute problem for low-γ nuclei since the magnitude of $\omega_1 = 2\pi\cdot\nu_1 = -\gamma B_1$ is proportional to the gyromagnetic ratio γ and thus large rf fields are harder to achieve.

It has recently been shown that with moderate ω_1, 'long' pulses of a rotor period or longer in duration can efficiently encode quadrupolar nuclei in heteronuclear correlation experiments.[11,12] These long pulses can bring crystallites with anisotropic frequency offsets into resonance with the rf pulse during brief level-crossings induced by the sample rotation.[11,13] Such a mechanism can cover transitions with large frequency spans even when the magnitude of the anisotropy is several orders larger than ω_1. Notably, frequency encoding becomes coherent when a pair of long pulses are used in a symmetric

National High Magnetic Field Laboratory, 1800 East Paul Dirac Drive, Tallahassee, FL 32310, USA. E-mail: hung@magnet.fsu.edu

† Electronic supplementary information (ESI) available. See DOI: 10.1039/d0cp04274a

manner as in the indirect ^{14}N dimension of ^{1}H/^{14}N HMQC pulse sequences.[11,13] Herein, this idea is extended to the STMAS experiment for half-integer quadrupolar nuclei to essentially remove the upper limit of quadrupolar interactions that are accessible and obtain isotropic spectra with high experimental efficiency.

Experimental section

All simulations were performed with SIMPSON,[14] using the pulse sequence in Fig. 1a and $t_1 = (2\pi/\omega_r) - (P1/2) - (P2/2)$, an asymmetry parameter $\eta_Q = 0$, MAS frequency of $\omega_r/2\pi = \nu_r = 16$ kHz,

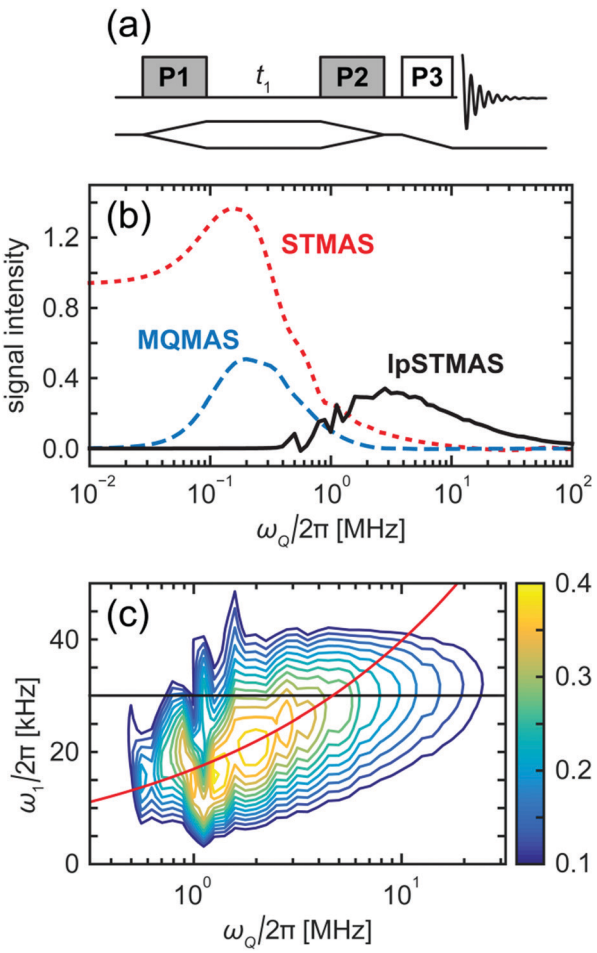

Fig. 1 Comparison of simulated $S = 3/2$ signal intensity for MQMAS, STMAS and lpSTMAS. (a) Three-pulse z-filter[15,16] sequence (P1–t_1–P2–ZF–P3–acq) used for SIMPSON[14] simulations. (b) Maximum signal for the MQMAS, STMAS and lpSTMAS experiments, as a function of ω_Q, normalized to CT-selective one-pulse direct-excitation spectra. The P1 and P2 rf field was fixed to $\omega_1/2\pi = 100$ kHz for MQMAS and STMAS, and $\omega_1/2\pi = 30$ kHz for lpSTMAS. All pulses were applied on-resonance with the CT, except the P1 and P2 pulses for lpSTMAS which were applied at an offset $\omega_{irr}/2\pi = +32{\cdot}\nu_r = +512$ kHz, where $\nu_r = 16$ kHz. (c) Contour plot of the lpSTMAS signal intensity as a function of ω_1 and ω_Q. The base contour level is set at an intensity of 0.1 and subsequent contours are at increments of 0.025. The horizontal black line denotes the position of the lpSTMAS curve shown in (b). The red curve highlights the optimal rf field dependence on the magnitude of the quadrupole coupling is approximately $\omega_1 \propto \omega_Q^{0.37}$.

and only first-order quadrupole coupling effects. The triple-quantum (3Q) transition was selected during t_1 for MQMAS, and the innermost $|\pm3/2\rangle \leftrightarrow |\pm1/2\rangle$ satellite-transitions (STs) were selected during t_1 for STMAS and lpSTMAS. The pulse sequence parameters for MQMAS were P1 = 6.7 μs, P2 = 1.5 μs, and a rf field of $\omega_1/2\pi = 100$ kHz; for STMAS P1 = 2.5 μs, P2 = 2.5 μs, $\omega_1/2\pi = 100$ kHz; for lpSTMAS P1 = P2 = $2\pi/\omega_r = 62.5$ μs are applied at an irradiation offset frequency $\omega_{irr}/2\pi = +32{\cdot}\nu_r = +512$ kHz. The P3 pulse was set equal to $0.5\pi/[\omega_1(S + 1/2)]$ in all instances with $\omega_1/2\pi = 10$ kHz.

All experiments were performed with Bruker Avance NEO spectrometers and double- or triple-resonance Low-E 3.2 mm MAS probes designed and built at the National High Magnetic Field Laboratory (NHMFL) in Tallahassee, FL, USA tuned to the CT frequency of all samples. ^{71}Ga spectra of β-Ga_2O_3 were recorded with the pulse sequences in Fig. S1 and $B_0 = 19.6$ T, $\omega_0(^{71}\text{Ga})/2\pi = 253.6$ MHz, $\omega_r/2\pi = 14.5$ kHz with a recycle delay of 3.5 s and 32 averaged transients. A one rotor-period spin-echo was appended to both the DQF-STMAS and lpSTMAS experiments before acquisition to avoid signal loss during the dead time. The spin-echo spectrum was acquired with P3 = 2.5 μs and P4 = 5.0 μs at $\omega_1/2\pi = 50$ kHz. The DQF-STMAS spectra were acquired with an initial $t_1 = (2\pi/\omega_r) - (P1/2) - (P2/2) - P4$, P1 = 2.7 μs and P2 = 2.5 μs at $\omega_1/2\pi = 110$ kHz, and P3 = 2.5 μs and P4 = 5 μs at $\omega_1/2\pi = 50$ kHz. The lpSTMAS spectra were acquired with an initial $t_1 = (2\pi/\omega_r) - (P1/2) - (P2/2) = 0$, P1 = P2 = $(2\pi/\omega_r) = 68.97$ μs at a power level equivalent to an on-resonance rf field of $\omega_1/2\pi = 55$ kHz, and P3 = 2.5 μs and P4 = 5 μs at $\omega_1/2\pi = 50$ kHz. All pulses were applied on-resonance with the central-transitions, except the P1 and P2 pulses for lpSTMAS which were applied at an offset $\omega_{irr}/2\pi = +36{\cdot}\nu_r = +522$ kHz, as optimized empirically for maximum overall signal. Any value of $\omega_{irr}/2\pi \sim 300$–$500$ kHz is a good starting point for experimental optimization of the P1 and P2 offset, though the lpSTMAS sensitivity does not depend critically on this parameter as long as ω_{irr} remains within the ST spinning sideband manifold without perturbing the CT. Though not strictly necessary, it is convenient to set the f_1 carrier frequency ($\omega_{irr}/2\pi$) equal to an integer multiple of ν_r. With a rotor-synchronized t_1, the ST peak positions appear as if the f_1 and f_2 carrier frequencies are the same. Additionally, during $\omega_{irr}/2\pi$ optimization, increments of ν_r should be used to avoid any modulations due to the shift between the apparent f_1 carrier frequency relative to that of f_2. The ^{71}Ga 2D lpSTMAS spectrum of β-Ga_2O_3 was acquired with a rotor-synchronized f_1 spectral width, 32 complex t_1 points, and 64 transients per t_1 point, resulting in a total experiment time of 4 hours. In particular, a first-order phase correction of -360° was applied in the indirect f_1 dimension during processing of the 2D spectra to account for the initial t_1 evolution, which is equal to $\tau_r = 2\pi/\omega_r$.

Results and discussion

Let us first examine the simulated sensitivity of the MQMAS and STMAS experiments for spin $S = 3/2$ nuclei. The three-pulse z-filtered pulse sequence used in simulations is shown in

Fig. 1a and the signal intensity of the two experiments as a function of ω_Q in Fig. 1b. With an rf field of $\omega_1/2\pi$ = 100 kHz for P1 and P2, the MQMAS experiment (Fig. 1b, blue dashed line) shows signal within a relatively narrow range of $\omega_Q/2\pi \sim$ 0.02–2 MHz (*i.e.*, $C_Q \sim$ 0.04–4.0 MHz). The theoretical maximum is ~0.5 when $\omega_Q/2\pi \sim$ 0.25 MHz, drops below 0.1 at $\omega_Q/2\pi$ = 1 MHz, and is essentially null above $\omega_Q/2\pi \sim$ 2 MHz. This is a severe limitation to MQMAS since samples with greater ω_Q values are commonplace and often of interest. To access larger ω_Q values an increase in ω_1 is necessary, but difficult to practically achieve, especially for low-γ nuclei. It is possible to increase the applied rf field by using probes with smaller coils, but the loss in sensitivity from the sacrifice in sample volume usually makes this venue counterproductive. Within the range of $\omega_Q/2\pi \sim$ 0.02–2 MHz, the simulation for STMAS generally shows similar rf behavior as MQMAS, but retains a sensitivity advantage of at least a factor of two (Fig. 1b, red dotted line). In fact, the STMAS signal around the optimal ω_Q value can exceed the signal of a direct-excitation spectrum because there are two STs that contribute to the signal, as opposed to a single central-transition (CT) observed with CT-selective direct-excitation. In addition, the simulation shows that higher $\omega_Q/2\pi$ values of up to ~5 MHz (*i.e.*, $C_Q \sim$ 10 MHz) may be accessible with STMAS. Simulations for other half-integer spin nuclei display similar behavior (Fig. S2, ESI†), though higher C_Q values can be accessed due to their higher spin quantum number S.

The present work proposes a straightforward revision of the three-pulse *z*-filter STMAS pulse sequence (Fig. 1a). Instead of using short, high-power pulses for ST excitation (P1) and conversion (P2), each pulse is lengthened in duration to one rotor period $\tau_r = 2\pi/\omega_r$, where $\omega_r = 2\pi\cdot\nu_r$ is the sample spinning frequency. In addition, the irradiation frequency (ω_{irr}) of the pulses is applied at a large offset in order to only excite the STs and minimize perturbation of the CT. The modified pulse sequence is denoted as low-power (lp) STMAS due to its lower rf field requirement compared to the conventional pulse sequence. A simulation applying P1 and P2 pulses of $\omega_1/2\pi$ = 30 kHz at an offset $\omega_{irr}/2\pi$ = +512 kHz with respect to the CT shows that lpSTMAS (Fig. 1b, black solid line) does not provide a sensitivity advantage over the optimal range of ω_Q for MQMAS and STMAS. However as ω_Q increases, the lpSTMAS signal becomes much higher than for MQMAS and STMAS, reaching a maximum of 0.35 at $\omega_Q/2\pi$ = 2.8 MHz and remaining above 0.1 at $\omega_Q/2\pi <$ 22 MHz. Thus, significantly expanding the range of ω_Q magnitudes for which isotropic spectra may be obtained. In addition, the lpSTMAS signal is relatively insensitive to changes in experimental parameters, displaying a broad maximum over a range of rf fields. As shown in Fig. 1c, the range of accessible ω_Q remains largely the same for $\omega_1/2\pi$ from 20 to 40 kHz with a relatively gradual loss of ~10–20% from changes in $\omega_1/2\pi$ of up to 15 kHz. In principle, the experiment can be extended to larger ω_Q by increasing both ω_1 and ω_{irr}, as shown in Fig. S3 (ESI†). Interestingly, simulations indicate that for $\omega_Q/2\pi$ from 1 to 300 MHz, the optimal rf field requirement increases very mildly at approximately $\omega_1 \propto \omega_Q^{0.37}$ as highlighted by the red curve in Fig. 1c.

Briefly, the theory for the rf spin dynamics which allows efficient ST encoding using long pulses is as follows. Large rf offsets from the STs during long pulses is modulated by MAS and can be treated in a jolting frame.[17] An average Hamiltonian can be obtained in the jolting frame as previously reported for the case of S = 1 nuclei,[11,13]

$$\bar{h} = \overline{\Delta\omega_Q} I_z + |s_n|\omega_1 e^{-i\varphi I_z} I_x e^{i\varphi I_z} \quad (1)$$

where $\overline{\Delta\omega_Q}$ is the offset of the nth spinning sideband (ssb) nearest to the rf irradiation frequency ω_{irr}, and s_n are Fourier expansion coefficients representing the ssb intensities for the STs under MAS. For the case of S = 3/2 nuclei, ω_{irr} is placed far off-resonance from the CT; thus, the two ST transitions can be treated as a pair of isolated two-level S = 1/2 systems. Given the number of ssbs, $\sim\omega_Q/\omega_r$, and the normalization condition, $\sum_n |s_n|^2 = 1$, eqn (1) shows that for pulses lasting τ_r, the amplitude of the rf Hamiltonian is scaled by the intensity of the nth ST ssb

$$|s_n| \sim \sqrt{\omega_r/\omega_Q} < 1 \quad (2)$$

and phase-shifted by φ, the phase of the complex intensity for the nth ssb nearest to ω_{irr}. That is to say, the effect of the rf field on each crystallite in a powder depends on the amplitude and phase of the MAS spectrum for that individual crystallite. Hence, application of a long rf pulse for excitation of a powder sample yields a magnetization which is not entirely coherent because of the rf phase variation among the different crystallites. Nevertheless, if a pair of such pulses is applied in the indirect dimension of two-dimensional experiments, such that their coherence order changes are equal in magnitude but opposite in sign, then the rf phase variation amongst the crystallites is cancelled between the pulses. More importantly, the large offset of the STs is reduced in the jolting frame to a small offset between ω_{irr} and the nearest ssb. Thus, efficient encoding of the STs is achieved using long pulses as shown in the simulations in Fig. 1. For a τ_r long pulse, the maximum encoding is obtained when $|s_n|\omega_1\tau_r = \pi/2$. From eqn (2), the optimal rf field for the lpSTMAS experiment is theoretically

$$\omega_1 \sim \frac{1}{4}\sqrt{\omega_Q\omega_r} \quad (3)$$

in qualitative agreement with the $\omega_1 \propto \omega_Q^{0.37}$ dependence seen in simulations. The square root dependence of ω_1 on ω_Q explains the low power requirement for the lpSTMAS experiment.

The performance of STMAS and lpSTMAS on a model compound with large quadrupolar interactions, β-Ga_2O_3, is shown in Fig. 2a. There are two inequivalent ^{71}Ga (S = 3/2) sites in β-Ga_2O_3, an octahedral (Ga^{VI}) and a tetrahedral (Ga^{IV}) site, which have C_Q values of 8.3 and 11.2 MHz.[18] The second-order quadrupolar broadening is much larger than the spinning frequency causing severe overlap of the ssbs even at a high magnetic field of 19.6 T. The 1D STMAS and lpSTMAS spectra are amplitude-modulated by their offsets in the indirect dimension due to the finite t_1 evolution equal to one rotor period between the P1 and P2 pulses. The lpSTMAS signal is surprisingly

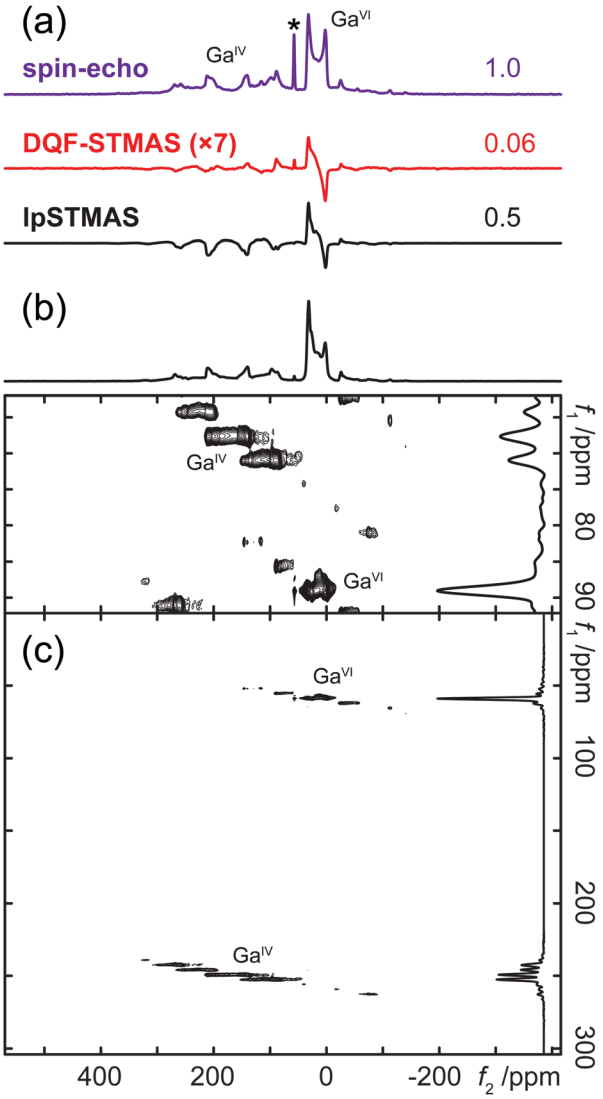

Fig. 2 (a) Experimental comparison of ^{71}Ga DQF-STMAS and lpSTMAS signal intensities with a spin-echo for β-Ga_2O_3. The vertical scale for the DQF-STMAS spectrum has been increased by a factor of seven to allow for easier visual comparison. The asterisk * denotes a sample impurity. 2D ^{71}Ga lpSTMAS spectrum after (b) isotropic shearing, and (c) Q-shearing,[22] expansion of the f_1 spectral width and shearing back into the isotropic representation to unravel spectral folding. The base contour level is set at 2% of the maximum intensity.

high compared to the 1D spin-echo spectrum at 0.5 for both Ga sites using a power level equivalent to an on-resonance rf field of $\omega_1/2\pi$ = 55 kHz, whereas the STMAS signal drops to 0.06 for Ga^{VI} and is almost undetectable for the Ga^{IV} site even with a much higher $\omega_1/2\pi$ of 110 kHz. The double-quantum filtered (DQF) STMAS[19] experiment was used for one-dimensional sensitivity comparisons in order to remove contributions from the large CT–CT autocorrelation signal. DQF-STMAS has been shown to retain ~80% of the signal compared to STMAS.[19] Thus, the estimated excitation and conversion efficiency of the STs using short, high-power pulses for STMAS is ~0.08. The lpSTMAS experiment is much less sensitive to the size of ω_Q and retains good efficiency without requiring very high rf fields, validating the theory and simulated results. Notably, no filtering elements are necessary to remove CT–CT autocorrelation signals for lpSTMAS. The ST excitation and conversion pulses (P1 and P2) were applied at a large offset of $\omega_{irr}/2\pi = +36\nu_r$ in order to minimize perturbation of the CT and therefore, the 1D lpSTMAS signal arises entirely from ST magnetization. The absence of any CT–CT signal is evidenced by the 2D lpSTMAS spectrum shown in Fig. 2b.

To the best of our knowledge, the ^{71}Ga nuclei in β-Ga_2O_3 have the largest quadrupolar interactions ($\omega_Q/2\pi$ = 4.15 and 5.6 MHz) for which high-resolution spectra have been reported,[20] as performed previously using DAS. Our attempts at obtaining an MQMAS spectrum resulted in only t_1 noise due to low efficiency. The conventional STMAS experiment also has much poorer sensitivity, where only the smaller C_Q Ga^{VI} site is discernible (not shown). These results are in good agreement with simulations, where STMAS has a slight advantage over MQMAS, but both experiments perform poorly for ω_Q values of these magnitudes.

The 2D lpSTMAS spectrum in Fig. 2b was acquired with rotor-synchronized t_1 evolution to avoid ssbs along the indirect dimension and improve the signal to noise ratio.[21] Rotor-synchronization restricts the indirect f_1 spectral width to $\omega_r/2\pi$ causing resonances farther than half the spectral width from the ω_{irr} of P1 and P2 to alias and not appear at their proper location in f_1, as observed in Fig. 2b. Higher MAS frequencies could be applied to alleviate some of the signal aliasing by providing a larger window in the indirect dimension. In the current instance, it is possible to resolve the aliasing by separating the two Ga signals using Q-shearing[22] (Fig. S4, ESI†). The spectrum can then be expanded in the f_1 dimension and sheared back to an isotropic representation to obtain a spectrum wherein the resonances are restored to their appropriate f_1 frequencies (Fig. 2c). A comparison of the spin-echo spectrum (Fig. 2a) and the isotropic spectrum (Fig. 2c, f_1 projection) illustrates the resolution enhancement achievable by lpSTMAS. The remarkable degree of overlap among ssbs in the direct dimension does not appear to have a significant deleterious effect on the ability of lpSTMAS to achieve high resolution in f_1 for this crystalline sample. In fact, the ssbs become clearly resolved in the 2D spectrum. Furthermore, the total intensities summed over the ssbs for the two sites are comparable in agreement with the presence of two equally populated crystallographic sites in the β-Ga_2O_3 crystal structure.[18,23] Once again emphasizing the ability of lpSTMAS to uniformly excite sites of significantly different C_Q values.

An additional benefit of the lpSTMAS experiment can be observed from its application to samples with smaller C_Q values, such as the ^{87}Rb nuclei of $RbNO_3$ (Fig. S5, ESI†), and ^{27}Al nuclei of $AlPO_4$-berlinite (Fig. S6, ESI†). Though in these cases lpSTMAS provides 20 to 40% less signal than conventional STMAS, the power requirement is also significantly lower, being equivalent to on-resonance $\omega_1/2\pi$ values of only 12 and 5.5 kHz for $RbNO_3$ and berlinite, respectively, compared to 80 and 71 kHz for the conventional high-power STMAS experiment. The low rf field requirement is of particular importance for low-γ nuclei for which large ω_1 are hard to

achieve, especially when large diameter rotors are used. Notably, the 2D ^{27}Al lpSTMAS spectrum of berlinite (Fig. S6, ESI†) also shows that the long-pulse excitation scheme is capable of selectively exciting only the innermost $|\pm3/2\rangle \leftrightarrow |\pm1/2\rangle$ STs without interference from higher-order $|\pm5/2\rangle \leftrightarrow |\pm3/2\rangle$ STs. Though excitation of high-order STs using τ_r long pulses is expected to be efficient, these coherences are only efficiently converted into lower-order ST polarization instead of the CT polarization typically observed during acquisition.

Conclusions

In summary, it has been shown by simulations and experiments that long pulses selective only to the STs can achieve much higher efficiency than short high-power pulses for STMAS of samples with large quadrupolar interactions. The new scheme dramatically reduces the requirement for high rf fields, thus greatly enhancing applicability to a variety of nuclei with large quadrupolar interactions and/or low gyromagnetic ratios. This advance opens up an entirely new regime of samples for which high-resolution isotropic STMAS spectra can potentially be obtained. It is hoped that researchers will see past the stringent but surmountable technical requirements necessary for STMAS-type experiments including lpSTMAS; primarily, accurate calibration of the magic-angle, so they may benefit from its rich information content.

Conflicts of interest

There are no conflicts to declare.

Acknowledgements

This work was supported by the National High Magnetic Field Laboratory (NHMFL) through NSF DMR-1644779 and the State of Florida. The NHMFL NMR facility is available to users free of charge. For more information please visit https://nationalmaglab.org/user-facilities/nmr-mri.

Notes and references

1 A. Samoson, E. Lippmaa and A. Pines, High-Resolution Solid-State NMR Averaging of 2nd-Order Effects by Means of a Double-Rotor, *Mol. Phys.*, 1988, **65**, 1013–1018.
2 A. Llor and J. Virlet, Towards High-Resolution NMR of More Nuclei in Solids - Sample Spinning with Time-Dependent Spinner Axis Angle, *Chem. Phys. Lett.*, 1988, **152**, 248–253.
3 L. Frydman and J. S. Harwood, Isotropic Spectra of Half-Integer Quadrupolar Spins from Bidimensional Magic-Angle-Spinning NMR, *J. Am. Chem. Soc.*, 1995, **117**, 5367–5368.
4 Z. H. Gan, Isotropic NMR spectra of half-integer quadrupolar nuclei using satellite transitions and magic-angle spinning, *J. Am. Chem. Soc.*, 2000, **122**, 3242–3243.
5 C. Huguenard, F. Taulelle, B. Knott and Z. Gan, Optimizing STMAS, *J. Magn. Reson.*, 2002, **156**, 131–137.
6 Z. Gan, P. Srinivasan, J. R. Quine, S. Steuernagel and B. Knott, Third-order effect in solid-state NMR of quadrupolar nuclei, *Chem. Phys. Lett.*, 2003, **367**, 163–169.
7 S. E. Ashbrook, S. Antonijevic, A. J. Berry and S. Wimperis, Motional broadening: an important distinction between multiple-quantum and satellite-transition MAS NMR of quadrupolar nuclei, *Chem. Phys. Lett.*, 2002, **364**, 634–642.
8 S. E. Ashbrook and S. Wimperis, High-resolution NMR of quadrupolar nuclei in solids: the satellite-transition magic angle spinning (STMAS) experiment, *Prog. Nucl. Magn. Reson. Spectrosc.*, 2004, **45**, 53–108.
9 J.-P. Amoureux, C. Fernandez and L. Frydman, Optimized multiple-quantum magic-angle spinning NMR experiments on half-integer quadrupoles, *Chem. Phys. Lett.*, 1996, **259**, 347–355.
10 Z. Gan, P. L. Gor'kov, W. W. Brey, P. J. Sideris and C. P. Grey, Enhancing MQMAS of low-gamma nuclei by using a high B-1 field balanced probe circuit, *J. Magn. Reson.*, 2009, **200**, 2–5.
11 I. Hung, P. Gor'kov and Z. Gan, Efficient and sideband-free ^{1}H-detected ^{14}N magic-angle spinning NMR, *J. Chem. Phys.*, 2019, **151**, 154202.
12 I. Hung and Z. Gan, High Resolution NMR of S = 3/2 Quadrupole Nuclei by Detection of Double-Quantum Satellite-Transitions via Protons, *J. Phys. Chem. Lett.*, 2020, **11**, 4734–4740.
13 A. J. Pell, K. J. Sanders, S. Wegner, G. Pintacuda and C. P. Grey, Low-power broadband solid-state MAS NMR of ^{14}N, *J. Chem. Phys.*, 2017, **146**, 194202.
14 M. Bak, J. T. Rasmussen and N. C. Nielsen, SIMPSON: A general simulation program for solid-state NMR spectroscopy, *J. Magn. Reson.*, 2000, **147**, 296–330.
15 J. P. Amoureux, C. Fernandez and S. Steuernagel, Z filtering in MQMAS NMR, *J. Magn. Reson., Ser. A*, 1996, **123**, 116–118.
16 Z. H. Gan, Satellite transition magic-angle spinning nuclear magnetic resonance spectroscopy of half-integer quadrupolar nuclei, *J. Chem. Phys.*, 2001, **114**, 10845–10853.
17 P. Caravatti, G. Bodenhausen and R. R. Ernst, Selective pulse experiments in high-resolution solid state NMR, *J. Magn. Reson.*, 1983, **55**, 88–103.
18 T. Vosegaard, I. P. Byriel, L. Binet, D. Massiot and H. J. Jakobsen, Crystal structure studies by single-crystal NMR spectroscopy. Ga-71 and Ga-69 single-crystal NMR of beta-Ga_2O_3 twins, *J. Am. Chem. Soc.*, 1998, **120**, 8184–8188.
19 H. T. Kwak and Z. H. Gan, Double-quantum filtered STMAS, *J. Magn. Reson.*, 2003, **164**, 369–372.
20 D. Massiot, I. Farnan, N. Gautier, D. Trumeau, P. Florian and P. Grandinetti, ^{69}Ga,^{71}Ga Solid-State Static, MAS and DAS NMR-Study of Beta-Ga_2O_3, *J. Chem. Phys. Biol.*, 1995, **92**, 1847–1850.
21 D. Massiot, Sensitivity and lineshape improvements of MQ-MAS by rotor-synchronized data acquisition, *J. Magn. Reson., Ser. A*, 1996, **122**, 240–244.
22 I. Hung, J. Trebosc, G. L. Hoatson, R. L. Vold, J. P. Amoureux and Z. Gan, Q-shear transformation for MQMAS and STMAS NMR spectra, *J. Magn. Reson.*, 2009, **201**, 81–86.
23 S. Geller, Crystal Structure of Beta-Ga_2O_3, *J. Chem. Phys.*, 1960, **33**, 676–684.